

DYNAMICAL EVOLUTION OF SPHERICAL AND CONICAL GRB REMNANTS

A. PANAITESCU & P. MÉSZÁROS

Dpt. of Astronomy & Astrophysics, Pennsylvania State University, University Park, PA 16802

ABSTRACT

We present an analytical approach to the dynamical evolution of fireballs or axially symmetric jets expanding into an external medium, with application to Gamma-Ray Burst remnants. This method leads to numerical calculations of fireball dynamics that are computationally simpler than hydrodynamic simulations. It is also a very flexible approach, that can be easily extended to include more complex situations, such as a continuous injection of energy at the reverse shock, and the sideways expansion in non-spherical ejecta. Numerical results for the dynamic evolution are discussed and compared to the analytical solutions. The light curves computed from beamed ejecta show that, due to the increased swept up matter and the time delay of the large angle emission, the sideways expansion of the remnant gas does not lead to a dimming of the afterglow, and mitigates the subsequent downturn from the transition into the non-relativistic regime.

Subject headings: gamma-rays: bursts - methods: analytical - radiation mechanisms: nonthermal

1. INTRODUCTION

Previous work on the dynamics of Gamma-Ray Burst (GRB) remnants was done analytically (Sari 1997, Vietri 1997, Chiang & Dermer 1998, Rhoads 1998, Wei & Lu 1998) or was based on hydrodynamical codes (Kobayashi, Piran & Sari 1998, Panaitescu & Mészáros 1998). The advantages and drawbacks of each of these approaches are evident: the former may not lead to sufficiently accurate results, but is more flexible and sometimes more powerful, while the second provides accuracy at the expense of substantial computational efforts, and may lack flexibility in including more sophisticated features. A fast but still sufficiently accurate computation of the remnant dynamics is necessary for calculations of the afterglow light-curves and spectra. Analytical treatments of the major afterglow features (Mészáros & Rees 1997, 1998, Vietri 1997, Waxman 1997, Wijers, Rees & Mészáros 1997, Mészáros, Rees & Wijers 1998, Panaitescu & Mészáros 1998, Rhoads 1998, Sari, Piran & Narayan 1998) have used asymptotic similarity solutions where the remnant Lorentz factor is a power-law in radius and the post-shock energy density is set by the Lorentz factor. In this work we further develop a more accurate and flexible semi-analytical approach presented by Panaitescu, Mészáros & Rees (1998) (PMR98). Our purpose is to obtain a method that leads to fast computations of remnant dynamics without making recourse to laborious hydrodynamic numerical codes, while retaining enough physical details to allow the calculation of the more important afterglow features.

2. REMNANT DYNAMICS

Model Assumptions and Features. We assume that, at any time during its evolution, the remnant is axially symmetric, i.e. there are no angular gradients in the shocked fluid, and all relevant physical parameters are functions only of the radial coordinate. This is equivalent to assuming that the initial energy distribution in the ejecta and the external gas are isotropic and that, in the case of a jet-like ejecta, the physical parameters of the remnant respond on a short time-scale to the effect of sideways expansion of the shocked gas. We also assume that the Lorentz

factor and the density within the shocked fluid can be taken as approximately constant. Otherwise, the model includes all other features developed so far in the literature: (i) delayed energy injection (Rees & Mészáros 1998), where for definiteness we shall use a power-law energy injection, (ii) an inhomogeneous external fluid (Vietri 1997, Mészáros et al. 1998); for simplicity we consider an external density which is a power-law in the radial coordinate, which includes the homogeneous and pre-ejected wind cases, and (iii) the above mentioned sideways expansion if the ejecta is not spherical (Rhoads 1998). Each of these features brings (or modifies) a specific term in the differential equations shown below, which give the evolution of the mass, kinetic and internal energy of the remnant.

External Medium. We consider an external gas whose density varies as a power-law with the radius: $\rho_{ex} = \rho_d(r/r_d)^{-\alpha}$. The natural length-scale is the deceleration radius r_d , defined as the radius at which the fastest (initial) part of the ejecta, moving with Lorentz factor Γ_0 , sweeps up an amount of external gas equal to a fraction Γ_0^{-1} of its own mass $M_0 c^2 = E_0/\Gamma_0$, i.e. $r_d = (3E_0/\Omega_0 n_d m_p c^2 \Gamma_0^2)^{1/3}$, E_0 being the energy of the leading ejecta, Ω_0 the solid angle of the cone within which it was released and n_d the external particle density at r_d . This is the radius at which the deceleration of the fireball by the interaction with the external gas becomes important.

The continuous interaction with the external gas increases the remnant mass

$$[dM]_{ex} = \Omega(r) \rho(r) r^2 dr, \quad (1)$$

where $\Omega(r)$ is the solid angle subtended by the it at radius r , which is larger than the initial Ω_0 due to the sideways expansion. The evolution of the half-angle θ of the remnant is $d\theta = c_s dt'/r$, where $c_s = c/\sqrt{3}$ is the comoving frame sound speed and $dt' = (\beta c \Gamma)^{-1} dr$ is the comoving time. Using $\Omega = 2\pi(1 - \cos \theta)$, the remnant solid angle evolves as

$$r(d\Omega/dr) = \sqrt{(\Omega/3)(4\pi - \Omega)/(\Gamma^2 - 1)}. \quad (2)$$

The interaction of the remnant with the external medium decelerates the remnant and heats it. Using energy and momentum conservation for the interaction between the remnant and

the infinitesimal swept-up mass $[dM]_{ex}$, one obtains that the comoving frame internal energy of the newly shocked gas is $(\Gamma - 1)$ times larger than its rest-mass energy, and the changes in the remnant internal U and kinetic K energies are given by

$$[dU]_{ex} = A(\Gamma - 1)c^2[dM]_{ex} , \quad (3)$$

$$[dK]_{ex} \equiv (Mc^2 + U)[d\Gamma]_{ex} = -(\Gamma^2 - 1)c^2[dM]_{ex} . \quad (4)$$

The multiplying factor A in the right-hand side of equation (3) was introduced to account for possible radiative losses in the shocked external gas, and represents the fraction of the internal energy of the shocked external gas that is not radiated away ($A = 0$ corresponds to a fully radiative remnant).

Delayed energy injection. As described by Rees & Mészáros (1998), we consider that the initial deposition of energy in the fireball (assumed to be short relative to the remnant dynamic timescale) is not uniform in the entire ejecta, in the sense that some parts of it have been given more energy and have been accelerated to higher Lorentz factors than other parts, which catch up with the faster ejecta as these are decelerated by the interaction with the surrounding medium. The entire process is fully characterized by the energy distribution $(dE/d\Gamma)_{inj}$ in the ejecta, at the end of the initial phase of acceleration, with all other relevant quantities resulting from the kinematics and energetics of the “catching up”. The Lorentz factor Γ_f of the delayed ejecta entering the decelerated part of the fireball moving with Γ is given by:

$$(d\Gamma_f/dr) = -(\beta_f\beta^{-1} - 1)(\Gamma_f^3\beta_f/ct) , \quad (5)$$

where r is the radial coordinate of the remnant, $t = c^{-1} \int_0^r (1 - \Gamma^{-2})^{-1/2} dr$ is the lab frame time, and $\beta = (1 - \Gamma^{-2})^{1/2}$ is the velocity corresponding to Lorentz factor Γ . Given the function $(dE/d\Gamma)_{inj}$, one can calculate the increase in the remnant kinetic and internal energies as result of the delayed injection, using energy and momentum conservation:

$$[dU]_{inj} = [\Gamma\Gamma_f(1 - \beta\beta_f) - 1]c^2[dM]_{inj} , \quad (6)$$

$$[dK]_{inj} \equiv (Mc^2 + U)[d\Gamma]_{inj} = \Gamma_f[1 - \Gamma^2(1 - \beta\beta_f)]c^2[dM]_{inj} , \quad (7)$$

where

$$[dM]_{inj} = \left(\frac{dE}{d\Gamma} \right)_{inj} \frac{|d\Gamma_f|}{\Gamma_f - 1} = F(\Gamma_f, \Gamma) M_{INJ} \frac{dr}{r} , \quad (8)$$

is the infinitesimal injected mass, $F(\Gamma_f, \Gamma)$ being a function that depends on the details of the delayed energy injection, and M_{INJ} the total mass of the delayed ejecta (see PMR98). In the numerical calculations we shall consider the particular case of a power-law injection: $(dE/d\Gamma)_{inj} \propto \Gamma_f^{-s}$ (Rees & Mészáros 1998) for $\Gamma_m < \Gamma_f < \Gamma_d$, where Γ_m and $\Gamma_d \equiv \Gamma(r = r_d)$ are the minimum and maximum Lorentz factors of the delayed ejecta.

Adiabatic Cooling. The delayed energy input at the reverse shock that moves into the incoming ejecta and the heating of the external fluid by the forward shock increase the internal energy of the remnant. This energy is lost adiabatically and radiatively. Unless the fraction of the energy given to the electrons by shock acceleration is above 10^{-1} and the fraction of

accelerated electrons is very small (i.e. $\lesssim 10^{-2}$, to maintain the electronic radiative phase for a long time), the radiative losses are small and the remnant can be considered adiabatic. If they were acting alone, adiabatic losses would accelerate the remnant, and in the presence of the external fluid, they ensure a continuous conversion of internal energy into kinetic energy, which mitigates the remnant deceleration. This is described quantitatively by

$$[dU]_{ad} = -(\hat{\gamma} - 1)(d_r V'/V')U , \quad (9)$$

$$[dK]_{ad} \equiv (Mc^2 + U)[d\Gamma]_{ad} = -\Gamma[dU]_{ad} , \quad (10)$$

where $V' = V'_{RS} + V'_{FS}$ is the comoving volume of the shocked ejecta (located behind the reverse shock) and of the swept-up external gas (behind the forward shock), and $\hat{\gamma} \sim 1.44$ is the adiabatic index of the remnant gas. In equation (9) $d_r V'$ denotes the infinitesimal variation of the comoving volume due only to the radial expansion of the gas, excluding the infinitesimal increases due to the addition of shocked fluid and to the sideways expansion (we neglect the adiabatic losses due to the sideways expansion, representing the acceleration of the outer parts of the fluid in the direction perpendicular to the radial direction of the flow). At this point we need a prescription for calculating the comoving volume V' and its radial variation $d_r V'$ (or the radial derivative of its logarithm). We consider two models for this: *Model 1*, where we assume that the lab frame increase in the thickness of the shocked fluid (external or delayed ejecta) is due only to the addition of new swept-up gas, and *Model 2*, where we assume that the comoving density of the two shocked fluids are uniform throughout each of the two sub-shells of injected ejecta and swept-up external gas, and have the values set by the shock jump equations.

MODEL 1. The assumption that the lab frame thickness of the already shocked fluid remains constant (i.e. that the thicknesses of the shells of shocked gases increase only due to the addition of new gas) implies that $d_r V'/V' = d(\Gamma r^2)/(\Gamma r^2)$, therefore

$$\frac{d_r V'}{V'} \stackrel{M1}{=} 2 \frac{dr}{r} + \frac{d\Gamma}{\Gamma} . \quad (11)$$

The comoving volume is $V' = \Omega r^2 \Gamma \Delta$, where Δ is the lab-frame thickness of the remnant, determined by the relative motion of the forward and reverse shocks: $d\Delta = (\beta_{FS} - \beta_{RS})dt$. The shock speed β_{RS} is calculated with a Lorentz transformation from β'_{RS} , the speed of the reverse shock measured in the frame of the incoming ejecta. The shock velocities β'_{RS} and β_{FS} are computed from the Lorentz factors $\Gamma' = \Gamma\Gamma_f(1 - \beta\beta_f)$ and, respectively, Γ of the shocked gases, as measured in the frame of the yet unshocked fluids, using the shock jump equations:

$$\beta'_{RS} = \frac{(\Gamma' - 1)(\hat{\gamma}\Gamma' + 1)}{\beta'\Gamma'[\hat{\gamma}(\Gamma' - 1) + 1]} , \beta_{FS} = \frac{(\Gamma - 1)(\hat{\gamma}\Gamma + 1)}{\beta\Gamma[\hat{\gamma}(\Gamma - 1) + 1]} . \quad (12)$$

MODEL 2. In this model, the two volumes V'_{RS} and V'_{FS} can be calculated from the masses of the shocked gases (eqs. [1] and [8]) and from the comoving densities, assumed to be uniform in each shell and having the same value as in the proximity of the shock. The comoving densities ρ'_{RS} and ρ'_{FS} behind the reverse and forward shock, respectively, are determined by the

comoving densities of the unshocked fluids, ρ'_f and ρ_{ex} , and by the Lorentz factors of the shocked gases, Γ' and Γ :

$$\rho'_{RS} = \frac{\hat{\gamma}\Gamma' + 1}{\hat{\gamma} - 1} \rho'_f, \quad \rho'_{FS} = \frac{\hat{\gamma}\Gamma + 1}{\hat{\gamma} - 1} \rho_{ex}. \quad (13)$$

Reverse Shock. The comoving density of the ejecta ahead of the reverse shock can be calculated by equating $[dM]_{inj}$ given by equation (8) with the mass $\Omega_f \Gamma_f \rho'_f r^2 dl$ swept up by the reverse shock as the remnant moves from r to $r + dr$, where $dl = ct|d\beta_f| = (\beta_f/\beta - 1)dr$ is the infinitesimal lab frame distance relative to the contact discontinuity covered by the reverse shock, and $\Omega_f(\Gamma_f, r)$ is the solid angle of the delayed ejecta, smaller than Ω , the solid angle of the decelerated remnant. Therefore, in general the isotropy assumption does not hold in the case of a beamed ejecta with delayed energy input, and the 1-dimensional model developed here for the delayed energy injection is appropriate only for spherical or large solid angle ejecta: $\Omega_f \sim \Omega \sim \Omega_0 \lesssim 4\pi$. The end result for ρ'_f is $\rho'_f = (\Gamma_f^2 \beta_f / 4\pi r^2 ct)(dM/d\Gamma)_{inj}$, so $V'_{RS} = (M_0 + \int_{r_d}^r [dM]_{inj})/\rho'_{RS}$ can be calculated by integrating equation (8) and using the first equation (13). From $d_r(\ln V'_{RS}) = -d(\ln \rho'_{RS})$ and equations (5) and (13), one can write

$$\frac{d_r V'_{RS}}{V'_{RS}} \stackrel{M_2}{=} G(\Gamma_f, \Gamma) \frac{dr}{r} + \frac{\hat{\gamma}\Gamma_f}{\hat{\gamma}\Gamma' + 1} \left(\frac{\beta_f}{\beta} - 1 \right) d\Gamma, \quad (14)$$

where $G(\Gamma_f, \Gamma)$ is a function of r and the details of the delayed injection.

Forward Shock. The volume of the shocked external fluid $V'_{FS} = (M_0/\Gamma_0 + \int_{r_d}^r [dM]_{ex})/\rho'_{FS}$ can be calculated using the second equation (13) and the swept-up mass obtained by integrating equation (1). From the second equation (13) it can be shown that

$$\frac{d_r V'_{FS}}{V'_{FS}} \stackrel{M_2}{=} \alpha \frac{dr}{r} - \frac{\hat{\gamma}}{\hat{\gamma}\Gamma + 1} d\Gamma. \quad (15)$$

Differential Equations for Remnant Dynamics. The remnant dynamics is given by the differential equations describing the evolution of the total kinetic and internal energies, coupled through the adiabatic losses:

$$dU = [dU]_{inj} + [dU]_{ad} + [dU]_{ex}, \quad (16)$$

$$dK \equiv (Mc^2 + U)d\Gamma = [dK]_{inj} + [dK]_{ad} + [dK]_{ex}, \quad (17)$$

where all quantities in the right-hand side terms are given by equations (3), (4), (6), (7), (9) and (10). Equations (16) and (17) include momentum and energy conservation, because the expressions of the terms that appear in it are derived using these conservation laws. By substituting the term $[dU]_{ad}$ from equation (17) in equation (16) ($[dU]_{ad}$ appears in the expression of $[dK]_{ad}$ – see eq. [10]), one arrives at $d[M(\Gamma - 1) + \Gamma U] = (\Gamma_f - 1)[dM]_{inj}$, which simply states that the net variation of the total energy of the adiabatic remnant equals the input of energy through the delayed injection (global energy conservation). With the aid of all the relevant equations previously derived, equations (16) and (17) can be written in a form that gives $d\Gamma/dr$ and dU/dr , respectively, i.e. the evolution of the flow Lorentz factor and of the co-moving internal

energy. These equations for the remnant dynamics are solved numerically together with equations (5) for Γ_f , (2) to find the jet solid angle, the equations for the two functions F and G (which were not shown explicitly), and the differential equation for the remnant mass resulting from equations (1) and (8):

$$r(dM/dr) = F(\Gamma_f, \Gamma)M_{INJ} + 3(\Omega/\Omega_0)(r/r_d)^{3-\alpha}(M_0/\Gamma_0). \quad (18)$$

The initial conditions for the set of differential equations for remnant dynamics are given by the values of the relevant quantities at $r = r_d$ (see PMR98): $\Gamma_f = \Gamma = 0.62\Gamma_0$, $U = 0.62 AM_0 c^2$, $M = (1 + \Gamma_0^{-1})M_0$, $\Omega \sim \Omega_0$.

3. NUMERICAL SOLUTIONS OF THE REMNANT DYNAMICS EQUATIONS

The analytical derivations above give prescriptions for calculating the evolution of the remnant Lorentz factor Γ and the internal energy U . The former determines the electron Lorentz factor, while the latter determines the magnetic field, both being necessary for the calculation of the afterglow light-curve and spectral evolution. As mentioned, it is customary in analytic derivations of afterglow light-curves to assume that the remnant Lorentz factor is a power-law in radius and to use the post-shock energy density set by the Lorentz factor to calculate all relevant quantities. The results thus obtained depend only on the assumed power-law for Γ . By contrast, here we are interested in solving the remnant differential equations in order to calculate the evolution of Γ with the observer time T ,

$$dT = \frac{1+z}{2\Gamma^2} dt = \frac{1+z}{2\Gamma\sqrt{\Gamma^2-1}} \frac{dr}{c}, \quad (19)$$

where z is the source redshift. Equation (19) gives the time when radiation emitted along the line of sight toward the observer arrives at Earth. Since we will focus mainly on adiabatic remnants, where the entire shocked gas contributes to the afterglow luminosity, it is not necessary to calculate the observer time using the Lorentz factor of the forward shock. A more accurate calculation of the time T should take into account the shape of the surface of equal arrival-time, i.e. the fact that most photons arriving at the detector are emitted from gas moving slightly off the line of sight toward the observer. This means that T given by equation (19) underestimates the "intensity-averaged" observer time by a factor $\lesssim 2$, for a relativistic remnant.

From the the expression of r_{dec} it is evident that the dynamics of the remnant is determined by $\varepsilon \equiv E_0/\Omega_0$, the energy per solid angle in the ejecta, and the parameters n_d and α characterizing the surrounding medium. The initial Lorentz factor Γ_0 is irrelevant (from the observer's point of view) for the dynamics of an adiabatic remnant running into a homogeneous external medium, because Γ_0 cancels out from the expression for $\Gamma(T)$ due to the $\Gamma \propto r^{-3/2}$ behavior encountered in this case. However, Γ_0 is an important parameter for a radiative remnant, or if the external medium is not homogeneous. The remnant dynamics is also determined by the parameters of the delayed energy injection, which for a power-law injection are Γ_m , Γ_0 , s and M_{INJ} (or, equivalently, the entire injected energy E_{INJ}), and by Ω_0 , the initial angular opening of the ejecta. The effect of the most important parameters can be assessed from Figures 1-3. In Figures 1-5, the solutions for the remnant dynamics obtained using *Model 1* are shown with shaded lines, while those obtained using *Model 2* are indicated with solid lines.

3.1. Spherical Remnants

Figure 1 shows the evolution of the radial derivative $d\Gamma/dr$ of the remnant Lorentz factor for a spherical remnant (i.e. no sideways expansion) with no delayed energy input, which is moving into a homogeneous external medium. The non-relativistic phase sets in at $r < 10r_d$ for a fully radiative remnant and at $r < 100r_d$ for an adiabatic one. This result is independent on the parameters ε and n_d , since we refer to the non-dimensional variable r/r_d , thus Γ as a function of r/r_d depends only on α , the index of the power-law external medium, and on Γ_0 . The derivative $d\Gamma/dr$ is expected to be equal to $(3 - \alpha)/(1 + A)$ (Mészáros et al. 1998), as long as the remnant is relativistic, and to depart from this value when the remnant enters the non-relativistic phase. Thus, if $\alpha = 0$, $\Gamma \propto r^{-3}$ for a radiative remnant and $\Gamma \propto r^{-3/2}$ for an adiabatic one. These analytic behaviors should hold for $r_d \ll r \ll \Gamma_0^{1/3} r_d$ if the remnant is radiative, and for $r_d \ll r \ll \Gamma_0^{2/3} r_d$ if it is adiabatic. The values of the exponents at early times, which are shown in Figure 1 and which were obtained from the numerical solution of the remnant dynamics differential equations, are consistent with the analytical expectations. Obviously, the numerical results are the same for both models of adiabatic losses, if the remnant is fully radiative. Due to the fact that for a radiative remnant the r^{-3} phase is short lived, this regime is not strictly reached for the case shown in Figure 1 ($\Gamma_0 = 500$), where the steepest Γ -decay attained is $\propto r^{-2.85}$. Only Lorentz factors $\Gamma_0 > 10^3$ allow this phase to fully develop at very early observer times ($T < 0.1$ day).

Figure 1 also shows that, for the same energy per solid angle in the ejecta, the quantity $-(d\Gamma/dr)$ falls below the above analytical value at earlier times for a radiative remnant than for an adiabatic one. Only in the radiative case the time of transition toward the non-relativistic phase depends on the initial Lorentz factor; this transition takes place later with decreasing Γ_0 . A larger energy in the ejecta also leads to a radiative remnant that remains relativistic for longer times. In the case of a pre-ejected wind ($\alpha = 2$), we obtained numerically the expected analytical exponents $-1/2$ (-1) for an adiabatic (radiative) remnant (these cases are not shown in Figure 1).

Figure 2 shows the effect of the delayed energy input on the dynamics of an adiabatic remnant, assuming a homogeneous external gas and a power-law distribution of energy per Lorentz factor in the delayed ejecta. The minimum Lorentz factor Γ_m of the ejecta determines the observer time when the injection ends. Prior to this time, the fireball Lorentz factor Γ decreases less steeply than in the case where there is no delayed injection. A very steep energy input (i.e. large parameter s), resembling the collision of a second shell with the leading fireball, may lead to a temporary flattening of Γ as a function of r , as shown by the small value of the derivative $d\Gamma/dr$ for $s = 10$, at $r \sim 2r_d$. The area of the expanding fireball visible to the observer increases as $(\Gamma T)^2$, while the intensity of its radiation at a frequency above the synchrotron peak evolves like $\Gamma^{6-4\beta}$, where β is the slope of the spectrum. Therefore, the flux from the remnant varies like $\Gamma^{8-4\beta} T^3$, which is $\Gamma^{12} T^3$ for $\beta = -1$ (the value observed for the afterglow of GRB 970508). This means that the afterglow corresponding to the remnant evolution shown in Figure 2 for $s = 10$ should exhibit a substantial brightening, with F_ν increasing as fast as T^3 at $T \sim 3$ days. The amplitude of the brightening is determined by the energy of the injected ejecta. One should distinguish between the implications of a

low value of $-(d\Gamma/dr)$ during the relativistic phase, due to the energy injection (resulting in a brightening of the afterglow), and a low value of the same quantity during the non-relativistic phase (resulting in an afterglow dimming). As shown in Figure 2, the differences between the solutions obtained with the two models for adiabatic losses are larger at times when most of the injection takes place, indicating that the adiabatic cooling of the shocked ejecta is the source of these differences.

3.2. Conical Remnants

For a jet-like remnant of small enough solid angle, it is possible that, before the remnant becomes non-relativistic, Γ drops below θ_0^{-1} and the observer sees the edge of the jet, which should in principle lead to a steepening of the light-curve decay because the emitting area no longer increases as $(\Gamma T)^2$, as it did when $\Gamma > \theta_0^{-1}$, remaining instead constant. The actual observed light curve, however, may be more complex than this, depending on the location of the observer relative to the jet axis and on the importance of sideways expansion (§4). The radius at which the above transition occurs can be estimated for an adiabatic remnant from

$$\Gamma = \Gamma_d (r/r_d)^{-3/2}, \quad (20)$$

whence the radius r_j at which $\Gamma(r_j) = \theta_0^{-1}$ is

$$r_j = (\Gamma_d \theta_0)^{2/3} r_d. \quad (21)$$

The remnant is still relativistic at r_j (i.e. $\Gamma \gtrsim 2$) if $\theta_0 \lesssim 1/2$ rad. If the jet is sufficiently narrow, then the sideways escape may have an important effect on the remnant dynamics and its afterglow decay before the onset of the non-relativistic phase. Using Rhoads' (1998) expression for the radius at which the sideways expansion becomes significant, we can write this as

$$r_b = [(75/8)\Gamma_0^2 \theta_0^2]^{1/3} r_d. \quad (22)$$

At the radius r_b the angular expansion of the ejecta has led to a net increase of the jet half-angle equal to the initial one, equation (22) being valid only if the remnant is still relativistic at r_b . Since the remnant Lorentz factor at r_b is $\Gamma_b = (2/5\sqrt{3})\theta_0^{-1}$ (Rhoads 1998), this condition reduces to $\theta_0 \ll 0.1$ rad $\sim 6^\circ$ ($\Omega_0 \ll 4 \times 10^{-2}$ sr). As shown by Rhoads (1998), during the sideways escape phase the remnant Lorentz factor Γ decreases as e^{-r/r_e} , with $r_e = (\Gamma_0 \theta_0)^{-2/3} r_d$ (nevertheless, the afterglow decay remains a power-law in the observer time). Thus during the exponential regime

$$[d \ln \Gamma / d(r/r_d)] = -(\Gamma_0 \theta_0)^{-2/3}. \quad (23)$$

Equations (21) and (22) show that $r_b/r_j \sim (75/4)^{1/3} \sim 2.7$, therefore the jet edge effect should always be seen before that of the angular expansion. From equations (19) and (20), one can show that $T \sim r/(2c\Gamma^2) \propto r^4$, therefore the ratio of the observer times at which the two transitions occur is $T_b/T_j = (r_b/r_j)^4 \sim 50$. Using the equation for r_{dec} , the times T_j and T_b can be calculated:

$$50 T_j = 3.8 [(1+z)/2] (\varepsilon_{54}/n_0)^{1/3} \Omega_{0,-3}^{4/3} [\text{day}] = T_b, \quad (24)$$

where ε_{54} is the initial energy per solid angle, in units of 10^{54} erg sr $^{-1}$, n_0 is the external medium number density in cm $^{-3}$ and $\Omega_0 = 10^{-3} \Omega_{0,-3}$ sr.

The dynamics of adiabatic conical or jet-like remnants is shown in Figure 3, assuming a homogeneous external medium. As indicated by equation (24), the evolution of Γ for such remnants depends on the parameters ε and Ω_0 . Figure 3 illustrates the fact that the exponential regime (i.e. the flattest part of each curve) is less evident for ejecta whose solid angle is close to or larger than the limit derived above of $\sim 10^{-1.4}$ sr, when the onset of the non-relativistic regime occurs before the sideways expansion has a significant effect on the remnant dynamics. From equation (24), the exponential regime is expected to start at $T_b \sim 4$ days for a jet energy $E_0 = 10^{51}$ ergs and at $T_b \sim 8$ days for $E_0 = 10^{52}$ ergs, in the case of the ejecta with the smallest solid angle shown in Figure 3, which is in agreement with the numerical results. For the same two cases, equation (23) predicts that during the exponential phase $-[d\Gamma/d(r/r_d)] = 0.23$ (for $\Gamma_0 = 500$), which is less than the value corresponding to the flattest parts of the dotted and dot-dashed curves in Figure 3 ($-[d\Gamma/d(r/r_d)] = 0.34 \pm 0.04$ for *Model 1* and 0.30 ± 0.04 for *Model 2*). Nevertheless the numerical and analytical results can be considered consistent with each other, given the approximations made in the derivation of equation (23).

4. SYNCHROTRON LIGHT-CURVES FROM BEAMED EJECTA

The observable effects arising from the beaming of the ejecta are illustrated in Figure 4. The calculation of the afterglow light-curve is described in PMR98, and consists in integrating the remnant emission over its entire evolution, over the infinitesimal layers of swept-up external gas, over the angle relative to the jet axis (required by the relativistic effects), and over the electron distribution. The electron distribution is determined by the assumed power-law distribution after shock acceleration and by the electron radiative and adiabatic cooling. The radiative cooling is due to synchrotron emission in a turbulent magnetic field. We assumed an electron index $p = 2.0$, and that electrons and magnetic fields acquire 10% of the post-shock internal energy. Figure 4a shows the light-curve seen by an observer located on the jet axis of symmetry. The points represent the observed R_c magnitudes for the afterglow of GRB 970508. With the exception of the latest two measurements, all data are from Sokolov et al. (1998). The initial energy per solid angle in the released ejecta is the same for all curves, only the jet initial half-angle is changed. The evolution of the afterglow brightness is identical until the time when the flow Lorentz factor has become sufficiently low that the observer “sees” the edge of the jet (i.e. the strength of the relativistic beaming of the radiation arriving at observer from the jet edge is not much below that of the relativistic beaming of the radiation emitted along the observer’s line of sight). This fact is illustrated by the $\theta_0 = 60^\circ$ and $\theta_0 = 20^\circ$ cases, where the sideways expansion is significant at times when the remnant is almost non-relativistic ($\Gamma \lesssim 2$). For $\theta = 10^\circ$, the jet edge is seen after $T_j^{lsc} \sim 3$ days (the superscript *lsc* specifies that this is the arrival time of the photons emitted by the gas which moves along the observer’s line of sight toward the center of explosion), while the transition to the non-relativistic phase and the sideways expansion occur at $T_{nr}^{lsc} \simeq T_b^{lsc} \sim 15$ days. The only cases shown in Figure 4a where the broadening of the jet is significant before the onset time of the non-relativistic phase are the $\theta = 4^\circ$ case, where $T_j^{lsc} \sim 0.3 \text{ d} < T_b^{lsc} \sim 2 \text{ d} < T_{nr}^{lsc} \sim 10 \text{ d}$, and the $\theta = 2^\circ$ case, for which $T_j^{lsc} \sim 0.03 \text{ d} < T_b^{lsc} \sim 0.3 \text{ d} < T_{nr}^{lsc} \sim 7 \text{ d}$. Note that in both these cases the light-curve does not steepen around

T_b^{lsc} or T_{nr}^{lsc} .

A clearer illustration of the effect associated with the broadening of the remnant jet is given in Figure 4b, where for comparison we show light-curves calculated with and without the increase of Ω according to equation (2). The jet has an initial half-angle $\theta_0 = 10^\circ$. For an observer located on the jet axis, the light-curves obtained with sideways expansion (thin solid curve) and without it (thin dotted curve) separate at $T \sim 3$ days, when the jet has a half-angle $\theta \sim 15^\circ$. The thin solid curve is obtained by integrating the remnant emission up to an angle $\theta = \theta_0$ relative to the central line of sight, i.e. up to a fixed angular opening equal to that of the initial opening of the ejecta (therefore it takes into account the sideways expansion in the dynamics, but not in the light-curve calculation of the radiation emitted by the fluid escaping outside the initial cone). This should be compared with the thick solid light-curve, where the remnant broadening is taken into account also in the integration of the radiation emission over angles, and with the dotted light-curve, where the sideways escape is suppressed (i.e. θ is maintained constant, at its initial value θ_0). The thin dotted and solid light-curves are obviously un-physical; we use them only to illustrate the factors at play in a broadening jet. As expected, the increase in the strength of the deceleration caused by the angular expansion of the jet diminishes the intensity of the radiation received from the fluid flowing within θ_0 of the jet axis. However, the radiation received from the fluid that has expanded to angles larger than θ_0 from this axis leads to an afterglow which is brighter than if the sideways escape were absent (thick solid curve versus dotted curve). The importance of the large angle emission can be assessed from the difference between the thick and thin solid curves in Figure 4b. This large angle emission is the cause of the absence of a break and dimming of the light-curve inferred analytically by Rhoads (1998) in connection with the sideways expansion of beamed GRB remnants. The analytical derivation of the light-curve presented by Rhoads (1998) assumed that the radiation emitted at some lab-frame time t arrives at the unique observer time T defined by equation (19) (this is the arrival time T_{lsc} corresponding of the radiation emitted by the fluid moving on the line of sight toward the center of explosion), thus neglecting the effects arising from the viewing geometry, due to the fast motion of the radiating fluid. Therefore, the sideways expansion delays the arrival time of part of the afterglow emission, prolonging its power-law decay rather than producing a break, as shown by the light-curves in Figure 4a, light-curves which steepen only due to the finite angular extension of the radiating fluid (as shown by the departures from the $\theta_0 = 60^\circ$ light-curve) and, with a less evident effect, by the transition to the non-relativistic regime.

Figure 4b also shows the effect of the jet orientation relative to the observer. Here, the observer is located at an angle $\theta_{obs} = 15.5^\circ$ relative to the jet axis, which has the same initial angle $\theta_0 = 10^\circ$ as before. Beside the effect described above related to the large angle emission, the sideways expansion also has the effect of bringing radiating gas onto the observer’s line of sight toward the origin $r = 0$, where the relativistic beaming is the strongest, thus leading to an even brighter emission compared to that which would be obtained in the absence of angular broadening (dashed versus long-dashed curves). In this case, by taking into account the viewing geometry, one reaches the conclusion that the sideways expansion produces a brighter afterglow. Figure 4b also shows the case where there is a delayed energy input (thick dot-dashed curve). This might in principle

explain the late time mild flattening of the GRB 970508 afterglow light-curve, even without invoking an underlying galaxy, implying that the decay would resume later on. The electron index used in this case was $p = 2.3$.

The spectral evolution of the afterglow from a conical remnant with $\varepsilon = 8 \times 10^{51} \text{ erg sr}^{-1}$, $\theta_0 = 10^\circ$, $\theta_{obs} = 15.5^\circ$, $p = 2.3$ and no delayed energy injection, using the two models for adiabatic losses, is shown in Figure 5. With our choice of the energy release parameters (i.e. electrons and magnetic field contain 10% of the internal energy), all the newly accelerated electrons of the power-law distribution electrons are radiative during the early afterglow ($T \lesssim 10$ days), and the peak of νF_ν is determined by the least energetic electrons of the power-law distribution. In the late afterglow ($T \gtrsim \text{few} \times 10$ days), the low energy end of the power-law distribution of the newly accelerated electrons is adiabatic. The νF_ν spectrum of the synchrotron radiation from these forward shock freshly injected electrons has a slope $(1/2)(3 - p)$ (positive for $p < 3$), corresponding to adiabatic electrons, up to the frequency at which the intermediate regime electrons radiate (i.e. the electrons whose adiabatic and synchrotron cooling timescales are equal), and a slope $(1/2)(2 - p)$ (negative for $p > 2$), corresponding to radiative electrons, above this frequency. Therefore, if $2 < p < 3$, the late time νF_ν spectrum of the radiation from freshly accelerated electrons should exhibit a shallow peak (the spectral slope changes by $1/2$) at the frequency at which the “transient” electrons radiate. This broad peak can be seen in the $T = 64$ and $T = 256$ days spectra shown in Figure 5. Notice that, if the energy release parameters do not change (as assumed here) when the remnant decelerates down to non-relativistic speeds, the synchrotron peak is still above few GHz at $T \gtrsim 100$ days. Also note that the optical and X-ray frequencies are above the spectral peak for $T > 1$ day, which implies that the electrons radiating at these frequencies are radiative.

5. DISCUSSION

We have presented an analytical model of the dynamics of an expanding fireball, capable of following the evolution from the onset the deceleration phase ($r \sim r_d$) until arbitrarily large times. The equations shown here are valid in any relativistic regime. The major assumptions underlying the analytical derivations are that, at any time, the remnant is axially symmetric (1-dimensional problem), and that the adiabatic cooling due to the sideways expansion is negligible compared with the cooling due to the radial expansion of the remnant.

This analytical treatment takes into account a possible delayed energy input resulting from an impulsive but uneven de-

position of energy in the ejected material. For non-spherical ejecta, it also takes into account the intensification of the remnant deceleration due to the increase in the solid angle of the remnant and, thus, in the rate at which it sweeps up external gas. The results presented in the previous section illustrate both of these effects. The treatment of the adiabatic losses require some assumption regarding the calculation of the remnant comoving volume. We considered two models for this: *Model 1* is based on the assumption that, if the accumulation of swept-up gas is subtracted, the remaining increase of the lab frame volume is due only to the r^2 increase of the remnant area; and *Model 2*, which is based on the assumption that the density profile in each of the two shells separated by the contact discontinuity is flat, implying that the comoving density tracks the density of the shocked fluid immediately behind the shock. The light-curves and spectra presented in Figures 4 and 5 for the two models for adiabatic losses do not differ by much.

The present approach has the advantage that it incorporates enough of the complexity of the dynamics of the ejecta and external medium interaction to allow reliable calculations of afterglow light-curves and spectra, without making use of the time-consuming iterative calculations involved in a hydrodynamical code. Therefore, our analytical method can be used to develop fast and very flexible numerical codes to calculate the afterglow dynamics and radiation. Such codes are necessary when one wants to perform model parameter searches. The *Model 2* presented in this work was used to simulate afterglow light-curves (Panaitescu, Mészáros & Rees 1998), in a version that did not include the adiabatic losses in the shocked ejecta nor the sideways expansion effect. Here, we presented light-curves arising from synchrotron emission from beamed ejecta, calculated using two models for the adiabatic losses, and assuming that the energy release parameters for the electron distribution and the magnetic field are constant down to non-relativistic velocities. Subject to these assumptions, the most important result is that the sideways expansion of beamed remnants does not produce a break and a dimming of the afterglow, but rather it extends the power-law decay to later times. This is due to the fact that the radiation emitted by the escaping fluid arrives later at the detector, smoothing the break that would be expected from analytical calculations, where the effects arising from the viewing geometry are not accounted for. Moreover, for narrow cone ejecta (see the $\theta_0 = 2^\circ$ and $\theta_0 = 4^\circ$ cases shown in Figure 4a), the sideways expansion iron out the light-curve break expected at the onset of the non-relativistic phase, the effect being weaker for ejecta with larger initial solid angle.

This research has been partially supported through NASA NAG5-2857 and NAG 3801.

REFERENCES

- Chiang, J. & Dermer, C. D. 1998, ApJ, submitted (astro-ph/9803339)
 Kobayashi, S., Piran, T. & Sari, R. 1998, ApJ, submitted (astro-ph/9803217)
 Mészáros, P. & Rees, M. J., 1997, ApJ, 476, 232
 Mészáros, P., Rees, M. J., & Wijers, R. 1998, ApJ, 499, 301
 Panaitescu, A. & Mészáros, P. 1998, ApJ, 501, in press (astro-ph/9711339)
 Panaitescu, A., Mészáros, P., & Rees, M. J. 1998, ApJ, 503, in press (astro-ph/9801258) (PMR98)
 Rees, M. J. & Mészáros, P. 1998, ApJ, 496, L1
 Rhoads, J. E. 1998, ApJ, submitted
 Sari, R. 1997, ApJ, 489, L37
 Sari, R., Piran, T., & Narayan, R. 1998, ApJ, 497, L17
 Sokolov, V. V. et al. 1998, A&A, 334, 117
 Vietri, M. 1997, ApJ, 488, L105
 Waxman, E. 1997, ApJ, 485, L5
 Wei, D. M. & Lu, T. 1998, ApJ, accepted (astro-ph/9712351)
 Wijers, R., Rees, M. J., & Mészáros, P. 1997, MNRAS, 288, L51

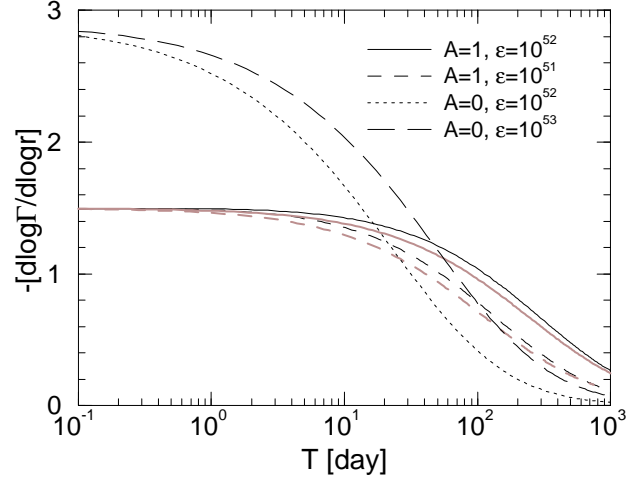


Fig. 1.— Evolution of $(d \log \Gamma / d \log r)$ for adiabatic ($A = 1$) and radiative ($A = 0$) spherical remnants, with no delayed injection and homogeneous external medium. Solid and dashed lines are for an adiabatic remnant, while dotted and long-dashed lines for a fully radiative one. The observer time T is calculated for $z = 1$, $n_d = 1 \text{ cm}^{-3}$ and $\varepsilon \equiv E_0 / \Omega_0$ as given in the legend, in units of erg sr^{-1} . Shaded curves correspond to *Model 1*, while solid lines are for *Model 2*.

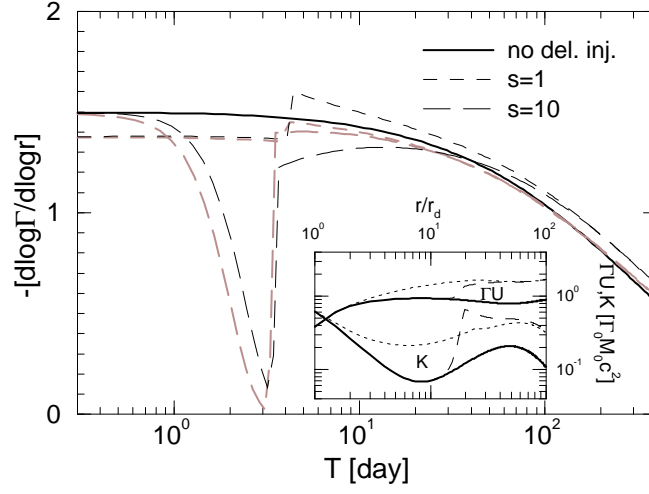


Fig. 2.— Effect of a power-law delayed energy input on the dynamics of an adiabatic spherical remnant interacting with a homogeneous external medium. The continuous curve is for the case with no delayed injection (added for comparison). The parameters of the injection are $\Gamma_m = 10$, $E_{INJ} = E_0$ and s is given in the legend. The inset shows the evolution of the kinetic and lab frame internal energy, in units of the initial remnant energy. Other parameters are: $z = 1$, $\varepsilon = 10^{52} \text{ erg sr}^{-1}$, $n_d = 1 \text{ cm}^{-3}$. As for Figure 1, *Model 1* solutions are shown with shaded lines, while *Model 2* solutions are indicated with solid curves.

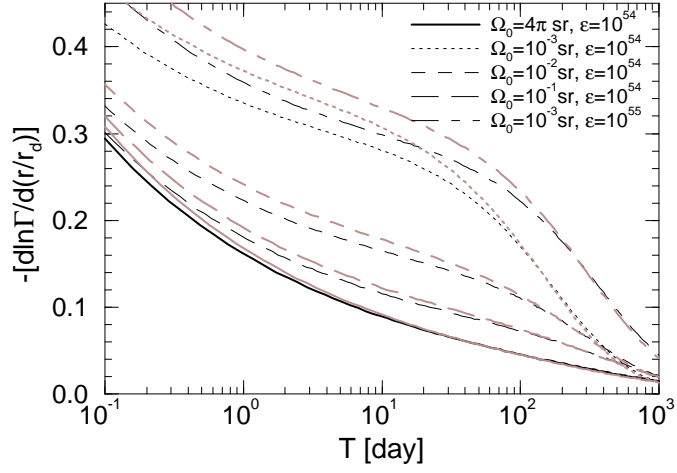


Fig. 3.— Evolution of $(d \ln \Gamma / dr)$ for adiabatic jet-like ejecta. The dynamics of such remnant depends on ε , the initial energy per solid angle (given in the legend in erg sr^{-1}), and on Ω_0 , the initial solid angle of the ejecta. Parameters: $z = 1$, $n_d = 1 \text{ cm}^{-3}$, $\alpha = 0$, $\Gamma_0 = 500$. The meaning of solid and shaded curves is the same as for Figures 1 and 2.

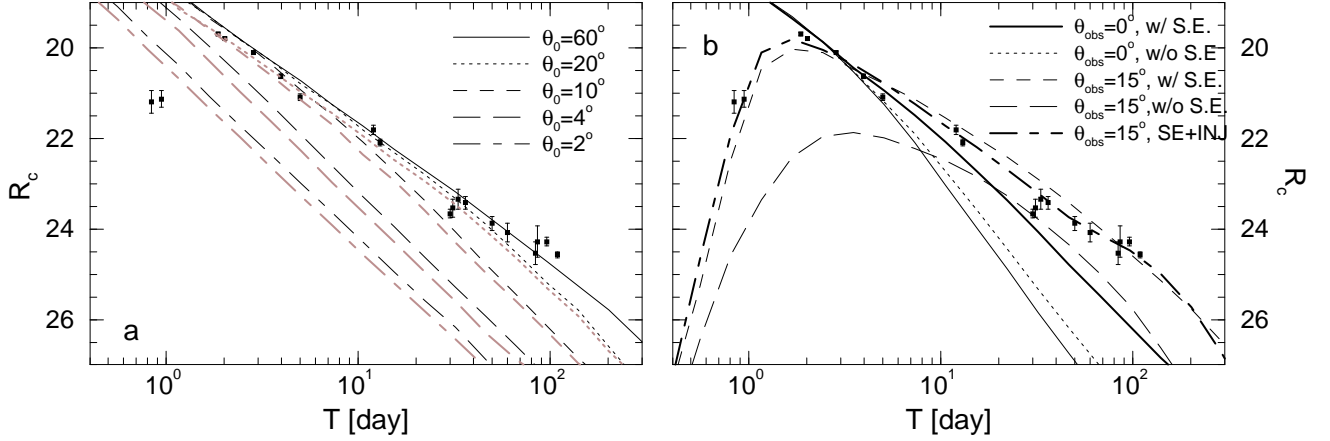


Fig. 4.— Optical light-curves and jet effects for beamed ejecta. The emission of radiation is calculated as described in PMR98 (see text for the relevant model parameters). The points represent observational data for the afterglow of GRB 970508; most of the data were taken from Sokolov et al. (1998). The shaded curves represent the R_c magnitude calculated with *Model 1*, while solid curves are for *Model 2*. Parameters: $z = 1$, $n_d = 1 \text{ cm}^{-3}$, $\alpha = 0$ and $\varepsilon = 2.5 \times 10^{51} \text{ erg sr}^{-1}$. The post-shock electron and magnetic field energy densities are each set to 10% of the internal energy density. Panel *a*: the observer is located on the axis of the jet, whose initial half-angle is given in the legend. Panel *b*: The effect of the sideways expansion for ejecta beamed into a cone that initially had a half-angle $\theta_0 = 10^\circ$, in two cases: the observer is on the jet axis ($\theta_{\text{obs}} = 0^\circ$) or at angle ($\theta_{\text{obs}} = 15.5^\circ$) relative to the symmetry axis. In the first case, $\varepsilon = 2.5 \times 10^{51} \text{ erg sr}^{-1}$ (same as in panel *a*), while in the latter $\varepsilon = 8 \times 10^{51} \text{ erg sr}^{-1}$. Note that in both cases, taking into account the sideways expansion leads to a brighter afterglow. The thick dot-dashed curve corresponds to a $\theta_0 = 10^\circ$ jet seen at 15.5° that has $E_0 = 7.6 \times 10^{50} \text{ ergs}$, corresponding to $\varepsilon = 8 \times 10^{51} \text{ erg sr}^{-1}$, and with a power-law delayed energy input characterized by $E_{\text{INJ}} = 0.5 E_0$, $\Gamma_m = 3$ and $s = 7$ (see text for details). For clarity, only light-curves obtained with *Model 2* are shown here.

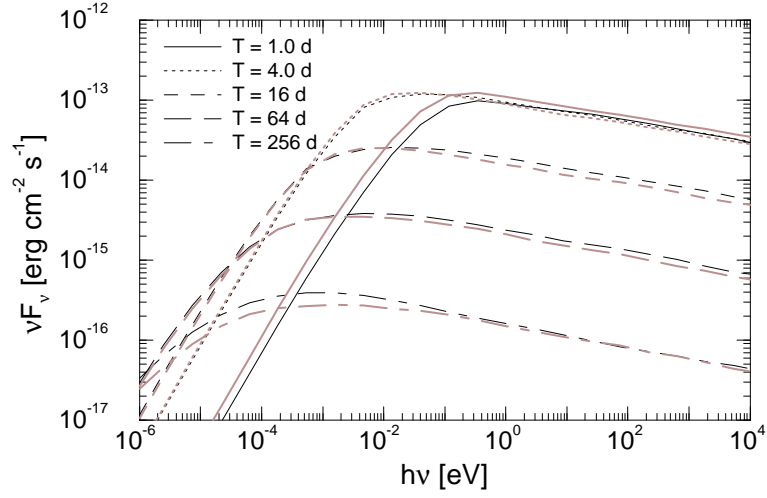


Fig. 5.— Spectral evolution of the synchrotron emission from ejecta beamed. The physical parameters are the same as for the remnant whose light-curve is shown in Figure 4b with thick dot-dashed line, except that here there is no delayed energy input. The electron index is $p = 2.3$, therefore the slope $-(p/2)$ of the spectrum above its peak is close to that observed in the afterglow of GRB 970508. Shaded curves: *Model 1*; solid curves: *Model 2*.